

First Principle Analysis of the Selective Ring Opening of Tetrahydrofurfural Alcohol  
over Rh surface

---

A Thesis

Presented to  
the faculty of the School of Engineering and Applied Science  
University of Virginia

---

in partial fulfillment  
of the requirements for the degree

Master of Science

by

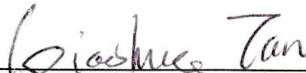
Qiaohua Tan

December

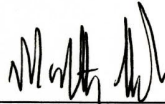
2012

APPROVAL SHEET

The thesis  
is submitted in partial fulfillment of the requirements  
for the degree of  
Master of Science

  
AUTHOR

The thesis has been read and approved by the examining committee:



Advisor





Accepted for the School of Engineering and Applied Science:



Dean, School of Engineering and Applied Science

December  
2012

## Abstract

The increasing demands for fuels and scarcity of petroleum resources have generated tremendous interest in the development of sustainable strategies that can convert biomass as well as other renewable feed sources into fuels and chemicals. Plant-based sugars and other biomass sources can be deconstructed into polyols and cyclic ether that contain excess oxygen which must be removed in the synthesis of useful chemical intermediates. In this work we carry out ab initio quantum chemical calculations to examine the plausible elementary reactions involved in hydrogenolysis of tetrahydrofurfural alcohol (*THFA*). The results are used to distinguish the possible mechanisms involved in the hydrogenolytic ring opening of *THFA* at the secondary carbon to form 1,2-pentanediol (*1,2-PDO*) and at the tertiary carbon to form 1,5-pentanediol (*1,5-PDO*). The results suggest that the C-H bonds of the methylene groups bound to the ether oxygen need to be broken in order to activate the C-O bond and open the ring. Coadsorbed hydrogen can assist in the activation of the C-O bond at the tertiary carbon center, however this was not the case for the activation of the C-O at the secondary carbon. The overall reaction path to form *1,5-PDO* was calculated to be less favorable than the path to form *1,2-PDO*, by about 20 kJ/mol, in agreement with experimental results of *THFA* hydrogenolysis on Rh/SiO<sub>2</sub>. The mechanistic insights from this work may be generalized to hydrogenolysis of a range of other cyclic ethers and polyols.

## Table of Contents

Abstract .....	3
Table of Contents .....	4
List of Figures .....	5
Chapter 1 - Introduction .....	7
Chapter 2 - Computational Methods .....	12
Chapter 3 - Results and Discussion .....	15
3.1 Overall Pathways.....	15
3.2 Hydrogenolysis of THFA to form 1,2-PDO .....	17
3.1 Hydrogenolysis of THFA to form 1,5-PDO .....	25
Chapter 4 - Conclusions .....	32
References .....	33
Appendix .....	39

## List of Figures

- Figure 1.** Schematic for the hydrogenolysis of *THFA* at different carbon centers leading to the formation of characteristically different products. .... 9
- Figure 2.** Hydrogenolysis of 1,2-dimethylcyclobutane on Rh catalysts towards 2,3-dimethylbutane and n-hexane. .... 10
- Figure 3.** Overall pathways for the hydrogenolysis of *THFA* to form *1,2-PDO* and *1,5-PDO*. Energetics for every elementary step are listed in kJ/mol ..... 16
- Figure 4.** Initial, transition and final state geometries for the dehydrogenation and ring opening reactions of *THFA* over the secondary carbon ..... 19
- Figure 5.** Reaction energy diagram comparing the direct single step ring-opening of the  $RC_sH-OR'$  (*Rxn 3*) shown in red to the three step path for the  $RC_s-OR'$  intermediate (*Rxns 2*→*5*→*13*) shown in black; the energies are reported in kJ/mol ..... 22
- Figure 6.** Energy diagrams for the four different pathways of the hydrogenation process from  $RC_s,OR'$  to *1,2-PDO* ..... 23
- Figure 7.** Most favorable potential energy path for the hydrogenolysis of adsorbed *THFA* at the secondary carbon to *1,2-PDO* over Rh(111) ..... 24
- Figure 8.** Initial, transition and final state structures for the dehydrogenation and ring opening reactions of *THFA* over the tertiary carbon ..... 26
- Figure 9.** Brønsted-Evans-Polyani relationship between the activation barriers and the overall reaction energies for the direct ring-opening of  $RC_s-OR'$ ,  $RC_sH-OR'$  and  $RO-C,R'$  intermediates (A) and the correlation of the of the activation energies for the direct ring opening and the H\*-assisted ring opening and the binding energies (B) of the three C-bound species  $RC_sH-OR'$ ,  $RC_s-$

*OR'* and *RO-C<sub>t</sub>R'* .....27

**Figure 10.** Most favorable potential energy path for the hydrogenolysis of adsorbed *THFA* at the tertiary carbon to *1, 5-PDO* over Rh(111).....30

**Figure A1.** Initial, transition and final states of the H assisted ring opening of the C-adsorbed species *RC<sub>s</sub>-OR'* and *RO-C<sub>t</sub>R'* .....38

**Figure A2.** Initial, transition and final state of the reactions involved in the hydrogenation of *RC<sub>s</sub>, OR'* towards *1,2-PDO* .....40

**Figure A3.** Initial, transition and final states of the elementary reactions involved in the hydrogenation of *RO, C<sub>t</sub>R'* towards *1,5-PDO* .....42

**Figure A4.** Reaction energy diagrams comparing the H assisted ring opening pathways and the direct ring opening pathways in the ring opening of the C-adsorbed species: (A) H-assisted ring opening of *RC<sub>s</sub>H-OR'* with H addition to carbon; (B) H-assisted ring opening of *RC<sub>s</sub>H-OR'* with H addition to oxygen; (C) H-assisted ring opening of *RC<sub>s</sub>-OR'* with H addition to oxygen; (D) H-assisted ring opening of *RO-C<sub>t</sub>R'* with H addition to carbon; (E) H-assisted ring opening of *RO-C<sub>t</sub>R'* with H addition to oxygen .....43

**Figure A5.** Reaction energy diagrams for the two different paths for the hydrogenation of *RO-C<sub>t</sub>R'* to form *1,5-PDO* .....44

## Chapter 1 – Introduction

The increasing demand for fuels and scarcity of petroleum resources has generated tremendous interest in the development of sustainable strategies that can convert biomass as well as other renewable feed sources into fuels and chemicals.<sup>1-8</sup> The most commonly studied biomass feedstocks are plant-based sugars that can produce various polyols and cyclic ethers that contain significant amounts of oxygen which make them unsuitable for fuels and undesirable as chemical intermediates.<sup>1,2</sup> The production of value-added chemicals from these feeds therefore requires catalytic processes that can selectively activate specific C-O bonds. Supported metal catalysts are often used in the hydrogenolysis of C-O bonds of alcohols.<sup>9-16</sup> For example, glycerol hydrogenolysis to form a mixture of diols has been studied over various supported-metal catalysts including Ru, Rh, Pt and Pd.<sup>9-14</sup>

While many studies have been presented on polyol hydrogenolysis, there are far fewer studies focused on the ring-opening hydrogenolysis of cyclic ethers. Tetrahydrofurfuryl alcohol (*THFA*) is an exemplary cyclic ether compound that can be easily produced from biomass.<sup>17</sup> The hydrogenolysis of *THFA* can proceed via the activation at the secondary C-O bond to form 1,2-pentanediol (*1,2-PDO*) or at the tertiary C-O bond to form 1,5-pentanediol (*1,5-PDO*), which are important monomers used in the synthesis of various polymers. As shown in Fig. 1, ring-opening at the secondary carbon leads to *1,2-PDO*, whereas the ring-opening at the tertiary carbon leads to *1,5-PDO*. *Koso, et al.*<sup>18</sup> examined the hydrogenolysis of *THFA* on Rh/SiO<sub>2</sub> in the presence as well as the absence of ReO<sub>x</sub> promoter and found that the ReO<sub>x</sub> promoter significantly increase the reactivity as well as the selectivity of the reaction. On the pure Rh catalyst, *1,2-PDO* is the

dominant product with 62% selectivity compared to 18% towards *1,5-PDO*, while on  $\text{ReO}_x$ -modified Rh catalysts, *1,5-PDO* was produced with 94% selectivity. It's apparent that over unmodified Rh, the metal-catalyzed hydrogenolysis of *THFA* appears to occur at the less-substituted carbon, whereas the  $\text{ReO}_x$  modifier shifts the selectivity towards activation at the more-substituted carbon. Due to well-known trends in the stability of carbenium ions, this shift suggests acid-catalyzed hydrogenolysis. In the recent publication by Chia, et al,<sup>19</sup> they showed the selective ring-opening of *THFA* as well as the analogous C6 cyclic ether, 2-(hydroxymethyl)tetrahydropyran, which also demonstrated a very high selectivity to activate at the more-substituted carbon over Rh- $\text{ReO}_x/\text{C}$  catalysts. The presence of acid sites in the Rh- $\text{ReO}_x/\text{C}$  catalysts was confirmed through ammonia TPD and the acid-catalyzed mechanism of ring-opening of *THFA* was elucidated. In contrast, the ring-opening of 2-methyltetrahydrofuran (*MTHF*) showed a rather different selectivity pattern with hydrogenolysis predominantly occurring at the less-substituted carbon on the same Rh- $\text{ReO}_x/\text{C}$  catalysts. The reaction rate, however, was found to be >30x lower than that of *THFA*. It was speculated that the low activity towards the formation of the less-substituted carbon was evidence that metal sites, rather than acid sites, were activating *MTHF*. This was supported by density functional theory (DFT) calculations which demonstrated that *MTHF* selectively ring-opens at the less-substituted carbon. While efforts continue to further understand the nature of acid sites of these  $\text{ReO}_x$ -promoted catalysts, the Rh metal can also still play a major role in the hydrogenolysis of the ether and, as stated, various others have focused on the hydrogenolysis over unpromoted supported metal catalysts. Thus, it becomes important to elucidate the mechanism of ring-opening hydrogenolysis over pure metal catalysts, to further understand both areas of research.

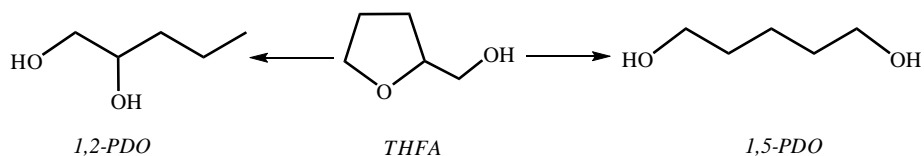


Figure 1. Schematic for the hydrogenolysis of *THFA* at different carbon centers leading to the formation of characteristically different products.

The selective hydrogenolysis of *THFA* and *MTHF* at the less-substituted carbon on pure Rh catalysts is similar to hydrogenolysis of cyclic hydrocarbons (such as methylcyclopentane and 1,2-dimethylcyclobutane) on Pt, Ni and Rh catalysts, which also favor activation at the less-substituted carbon.<sup>20-29</sup> The hydrogenolysis of 1,2-dimethylcyclobutane on Rh film produces 91% 2,3-dimethyl-butane, which indicates the selective breaking of the less-substituted C-C bond as shown in Fig. 2.<sup>25</sup> This selective C-C cleavage was reported to proceed by the initial scission of the four hydrogen atoms to form the  $\alpha,\alpha,\beta,\beta$ -tetra-adsorbed intermediate prior to C-C bond activation.<sup>24-27</sup> Although 1,2-dimethylcyclobutane primarily activates at the less-substituted C-C bonds, the rate of C-C cleavage at the more-substituted carbon can be affected by the stereochemistry of the C-C bond. It was found that higher yields of n-hexane and 3-methylpentane were formed from the *cis*- isomer rather than from the *trans*- isomer as shown in Fig. 2. Before cleavage of the substituted C-C bond, an  $\alpha,\beta$ -diadsorbed species is believed to be formed by elimination of two H atoms and the steric interaction of the substituted methyl group with the surface hinders the dehydrogenation from the *trans*- isomer.<sup>28-29</sup> Both of these examples for the hydrogenolysis of cyclic hydrocarbon suggest that prior to C-C activation, C-adsorbed species are formed by the elimination of H atoms, and the dehydrogenation across the C-C bond is associated with the selectivity of the C-C activation.

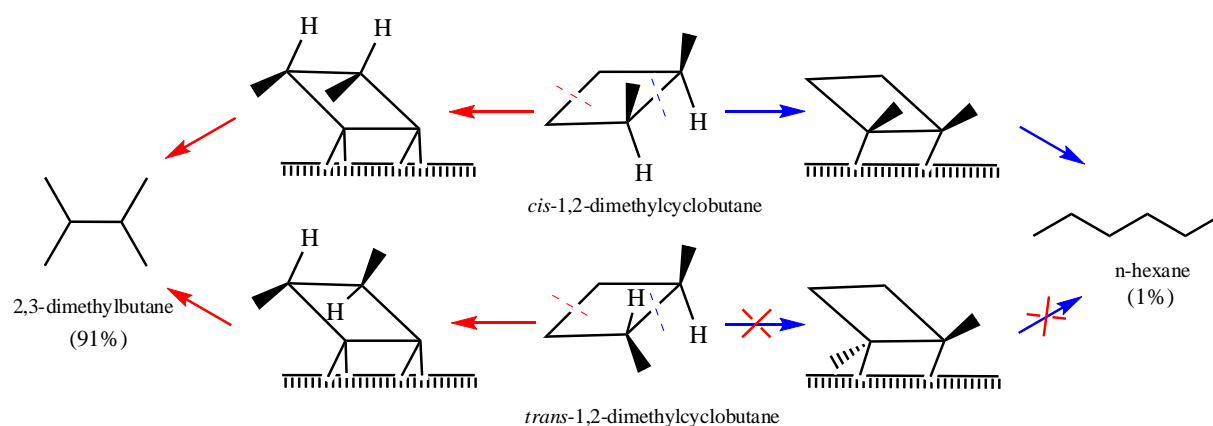


Figure 2. Hydrogenolysis of 1,2-dimethylcyclobutane on Rh catalysts towards 2,3-dimethylbutane and n-hexane.<sup>28, 29</sup>

Similar dehydrogenation pre-requisites have also been reported for C-C and C-O bond hydrogenolysis of monofunctional alcohols and polyols. The hydrogenolysis of glycerol over supported Ru catalysts, for example, is thought to proceed by the dehydrogenation of glycerol to glyceraldehyde prior to C-O or C-C scission.<sup>12,16</sup> Compared with the cyclic hydrocarbon hydrogenolysis mechanisms, glyceraldehyde can be considered to be an  $\alpha,\beta$ -diadsorbed species formed via the dehydrogenation of C-O bond. Similar behavior has also been observed by Gennari, *et al.* in a study of hydrogenolysis of *MTHF* over Pt catalysts in which chemisorption of hydrogen from the ether carbon was detected by IR methods, and as well higher selectivity over the less-substituted carbon of *MTHF* was found.<sup>30,31</sup>

Based on the previous insights into the hydrogenolysis mechanisms that control the C-C and C-O activation of linear alcohols such as glycerol as well as cyclic ethers which include *MTHF*, we propose that during the hydrogenolysis of *THFA*, one or more of the C-H or O-H bonds are broken in order to form a dehydrogenated and more strongly bound intermediate which will

readily go on to activate the C-O or C-C bond breaking. The resulting intermediate will likely hydrogenate to form the final diol products. However, the exact nature of the mechanism and what determines product selectivity is still rather unclear.

In this work we carry out first-principle density functional theoretical calculations to examine the elementary steps and explore plausible reaction pathways for the hydrogenolysis of *THFA* over the Rh (111) surface and thus gain insights into the mechanisms that control ring-opening hydrogenolysis of cyclic ethers over noble metal catalysts.

## Chapter 2 - Computational Methods

All of the calculations in this study were carried out using periodic plane wave gradient-corrected density functional theory methods implemented in the Vienna ab initio Simulation Package (VASP) codes developed by Kresse and Hafner.<sup>32</sup> A plane wave basis set with a cut off energy of 400 eV was used to describe the electronic structure for each of the ions and to solve the series of Kohn-Sham equations.<sup>33</sup> The PW91 form of generalized gradient approximation (GGA) exchange correlation functional was used to provide the non-local gradient-corrections to exchange and correlation energies.<sup>34</sup> Ultrasoft pseudopotentials were used to describe the Kohn Sham orbitals in the core region.<sup>35</sup> The wave functions and charge density were converged to within  $10^{-6}$  eV. The geometric structures for all calculations were optimized until the forces were converged to within 0.05 eV/Å using a  $3\times 3\times 1$  k-point mesh to sample the first Brillouin zone.<sup>36</sup> The energies of the optimized structures were then calculated with a  $6\times 6\times 1$  k-point mesh to integrate over the first Brillouin zone. The convergence criteria of 0.05 eV/Å was verified by further optimizing a set of structures presented in this paper to a convergence criteria of 0.01 eV/Å. This tighter convergence criteria resulted in changes to the overall energy of  $< 0.02$  eV, which is believed to be smaller than the intrinsic error in the method.

The nudged elastic band (NEB) method<sup>37-40</sup> was used to find reaction pathways by linearly interpolating 16 images between the initial and final states and then minimizing the energy of the string of images until the forces perpendicular to the reaction path converged within 0.25 eV/Å. Then initial guess of the transition state and reaction mode were grabbed from the minimum energy path for further locating the transition state by dimer method.<sup>41-43</sup> The dimer methods

works with two images as the ‘dimer’ which are slightly displaced by a fixed distance. The transition state was located by moving the ‘dimer’ uphill on the potential energy surface along which the ‘dimer’ is rotated in order to keep the lowest curvature mode of the potential energy. The dimer calculations were converged until the forces perpendicular to the reaction mode were beneath 0.05 eV/ Å, that geometry was then calculated at a 6x6x1 k-point mesh as described above.

A 3x3 Rh (111) surface with four metal layers and 15 Å of vacuum separating slabs in the z-direction was used for all of the reported calculations. In order to establish the intrinsic reactivity we examine the low coverage regime of 1/9 ML of adsorbed *THFA* and 1/9 ML of adsorbed atomic hydrogen. The top two metal layers were allowed to relax in the calculations whereas the bottom two layers were held fixed to their bulk position. The optimized bulk Rh lattice constant is calculated to be 3.80 Å which is in agreement with the experiments.<sup>44</sup> The energies of the adsorbates in vacuum were calculated spin-polarized in an 18×18×18 Å unit cell.

The binding energies of the surface species were calculated as:

$$E_{ads} = E_{surf+ads} - E_{surf} - E_{ads}$$

where  $E_{surf+ads}$  is the total energy of the metal surface with the adsorbate bound to the metal,  $E_{surf}$  is the total energy of the bare metal surface and  $E_{ads}$  is the total energy of the adsorbate in gas phase.

The activation barriers and reaction energies were calculated as:

$$E_{ACT} = E_{TS} - E_R$$

$$E_{RXW} = E_P - E_R$$

respectively where  $E_{TS}$  is the total energy of the transition state,  $E_R$  is the total energy of the reactant state and  $E_P$  is the total energy of the product state. For  $E_R$  and  $E_P$ , if more than one species is adsorbed on the surface, they are calculated as:

$$E_R \text{ or } E_P = E_{surf++1^+} E_{surf++2^+} \cdots E_{surf++n^-} (n - 1) E_{surf}$$

where  $E_{surf+1}$  is the total energy of the metal surface with adsorbed species 1 and similarly  $E_{surf+2}$  and  $E_{surf+n}$  are the total energies of the metal surface with adsorbed species 2 and species  $n$  with the assumption that there are no interactions between species .

## Chapter 3 - Results and Discussion

### 3.1 Overall Pathways

The various possible pathways for the ring opening and hydrogenolysis of *THFA* at both the secondary and more-substituted tertiary C-O bonds are shown in Fig. 3. The secondary carbon (represented by  $C_s$  here) of *THFA* has two H atoms and can therefore result in two potential C-adsorbed dehydrogenated intermediates:  $RC_sH-OR'$  which results from breaking one of the C-H bonds and  $RC_s-OR'$  which occurs via the scission of both C-H bonds, while only one C-adsorbed intermediate ( $RO-C_tR'$ ) results from the activation of the C-H bond on the more substituted tertiary carbon (represented by  $C_t$  here) as only one C-H bond is present.

The activation of the C-H bonds leads to more strongly held intermediates to the surface and initial weakening of the neighboring C-O bonds which helps ring-opening C-O bond scission. The activation of the C-O bond can occur directly on the surface or may be assisted by adsorbed hydrogen which is present under hydrogenolysis conditions. As such we examine both the direct and H-assisted C-O activation over the metal surface. The resulting C- and O- bound ring-opened intermediates that form upon C-O activation are subsequently hydrogenated to form the *1,2-PDO* or *1,5-PDO* products. Depending on the intermediate that forms upon ring-opening, two or four hydrogen addition steps will be required to form the diol products. The order of the H-addition steps will lead to the formation of different intermediates and as such different pathways. The activation and reaction energy for all the elementary steps that make up these paths were calculated and shown in Fig. 3. We discuss in more detail each of the different pathways and mechanisms involved in the hydrogenolysis of *THFA* to *1,2 PDO* and *1,5 PDO* in

the two subsections that follow.

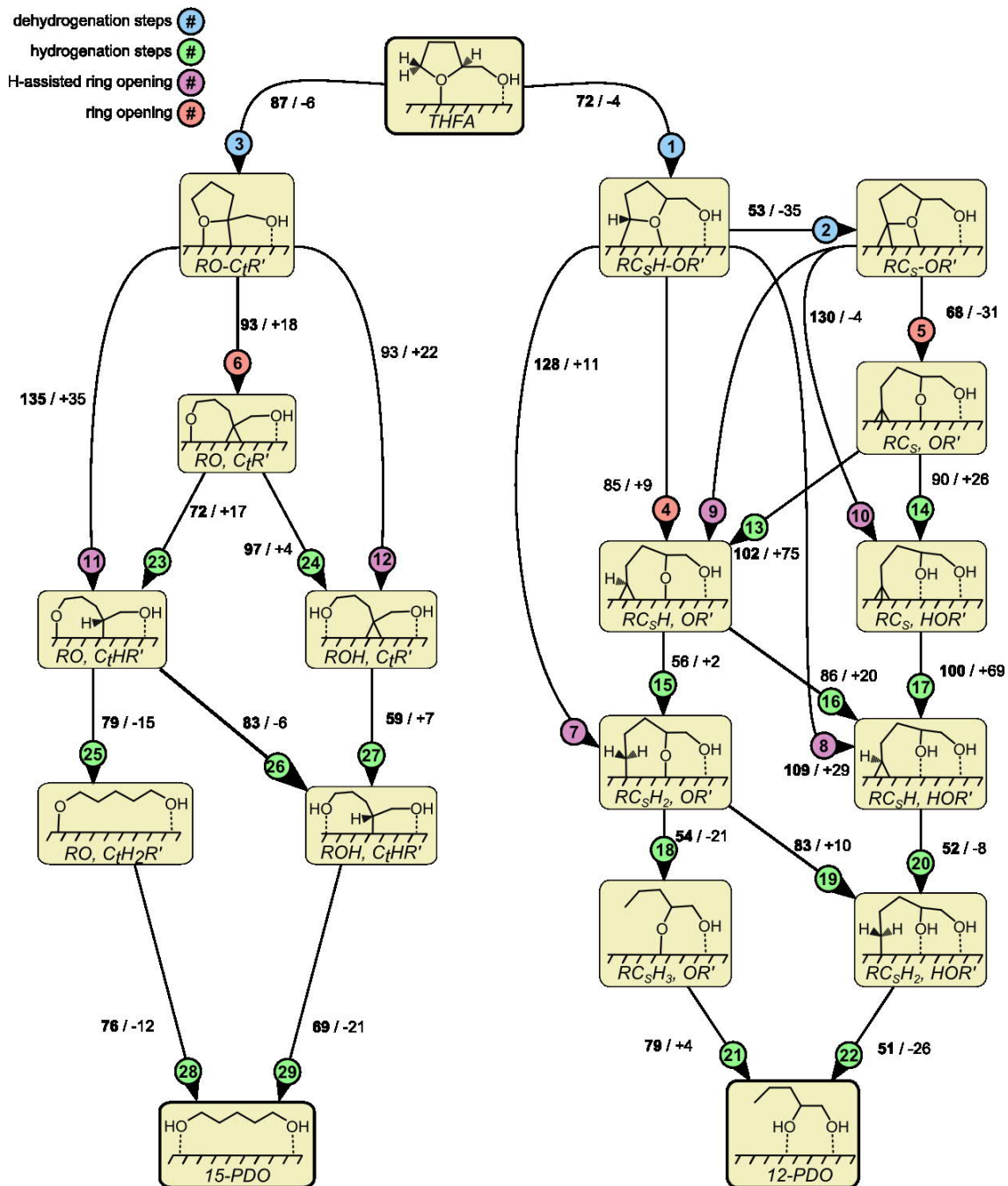


Figure 3. Overall pathways for the hydrogenolysis of THFA to form 1,2-PDO and 1,5-PDO.

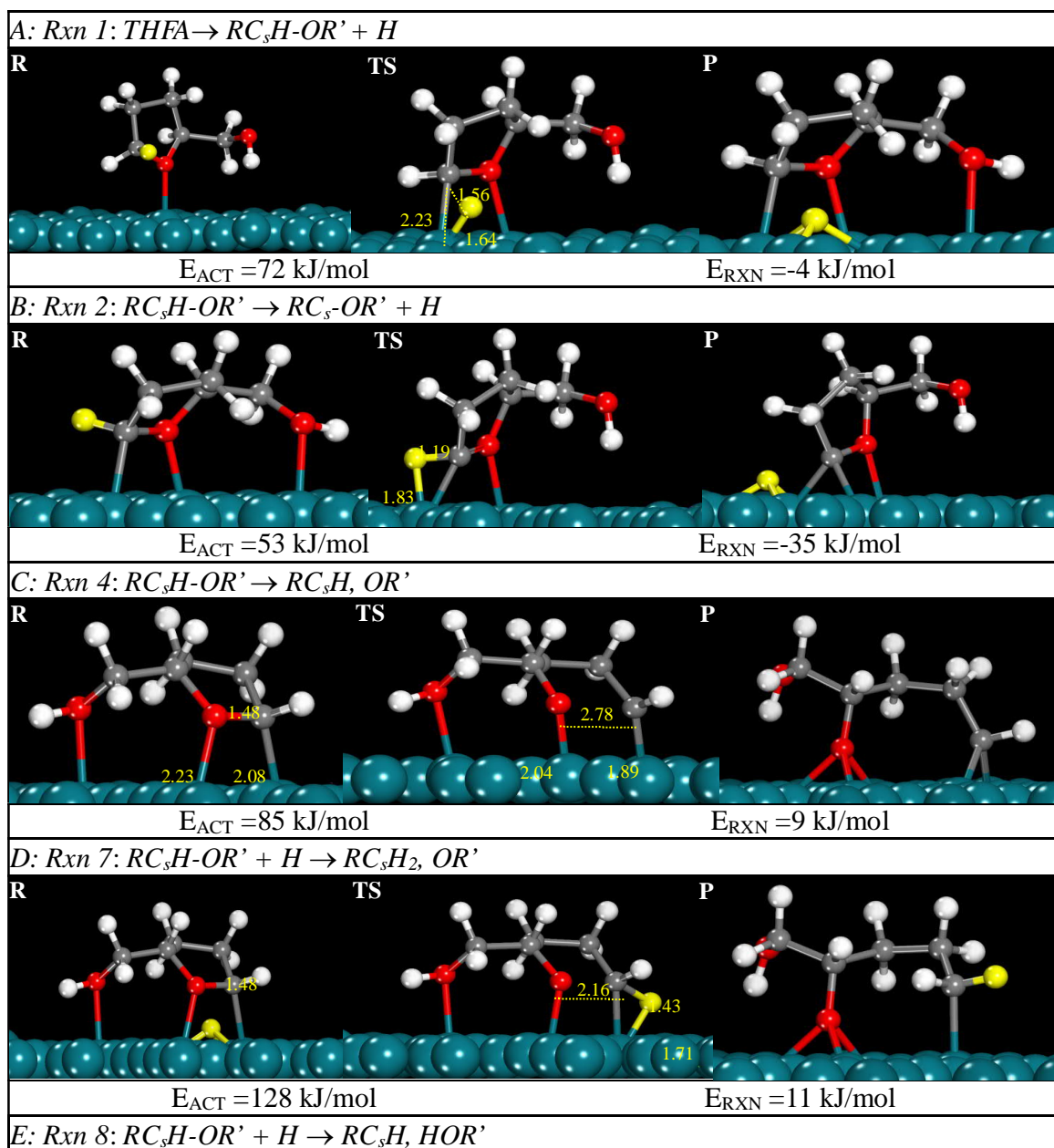
Energetics for every elementary step is listed in the unit of  $kJ/mol$ .

### 3.2 Hydrogenolysis of THFA to form 1,2-PDO

THFA adsorbs on the Rh surface through its ether oxygen atop a metal center with the distance of 2.30 Å and tilted away from the surface normal by an angle of 40 degrees. This mode is characteristic for the adsorption of water and other alcohols as the binding involves the donation of a non-bonding lone pair of electrons on the oxygen into the metal<sup>45-46</sup> and results in an adsorption energy here of -44 kJ/mol. It's important to note that in this mode of adsorption the hydroxyl group could not bind to the surface due to structural constraints. The initial, transition and final state structures for the reaction involving the scission of the first C-H bond at the secondary carbon to form  $RC_sH-OR'$  intermediate is shown in Fig. 4A (*Rxn 1*). The reaction starts with a rotation around the ether oxygen of the adsorbed THFA, such that the C-H bond of the secondary ether carbon is oriented toward a surface metal atom to allow for C-H activation. The reaction proceeds via metal atom insertion into the C-H bond with the C-H distance elongated from 1.10 Å to 1.56 Å in the transition state, which is characteristic for C-H activation reactions for other hydrocarbons.<sup>47-48</sup> The reaction is slightly exothermic with the reaction energy of -4 kJ/mol. The activation energy is calculated to be 72 kJ/mol, which is consistent with the terminal C-H activation barrier of 74 kJ/mol reported for glycerol on Rh (111).<sup>47</sup>

At this point, the  $RC_sH-OR'$  intermediate can either ring open as discussed below, or continue to dehydrogenate by activating the 2<sup>nd</sup> C-H from the secondary carbon, forming a bridge-bound carbon intermediate ( $RC_s-OR'$ ). As shown in Fig. 4B (*Rxn 2*), the 2<sup>nd</sup> C-H activation of  $RC_sH-OR'$  also proceeds via the classic oxidative metal atom insertion into the C-H bond as the C-H distance increases from 1.10 Å to 1.19 Å in the transition state. It is noted that the C-O bond distance decreases from 1.48 Å to 1.41 Å as a result of the double bond that forms between the

two. The elimination of the 2<sup>nd</sup> H atom is exothermic at -35 kJ/mol and has an activation barrier of 53 kJ/mol. We can see that the elimination of the 2<sup>nd</sup> hydrogen atom is much easier than the 1<sup>st</sup> hydrogen atom.



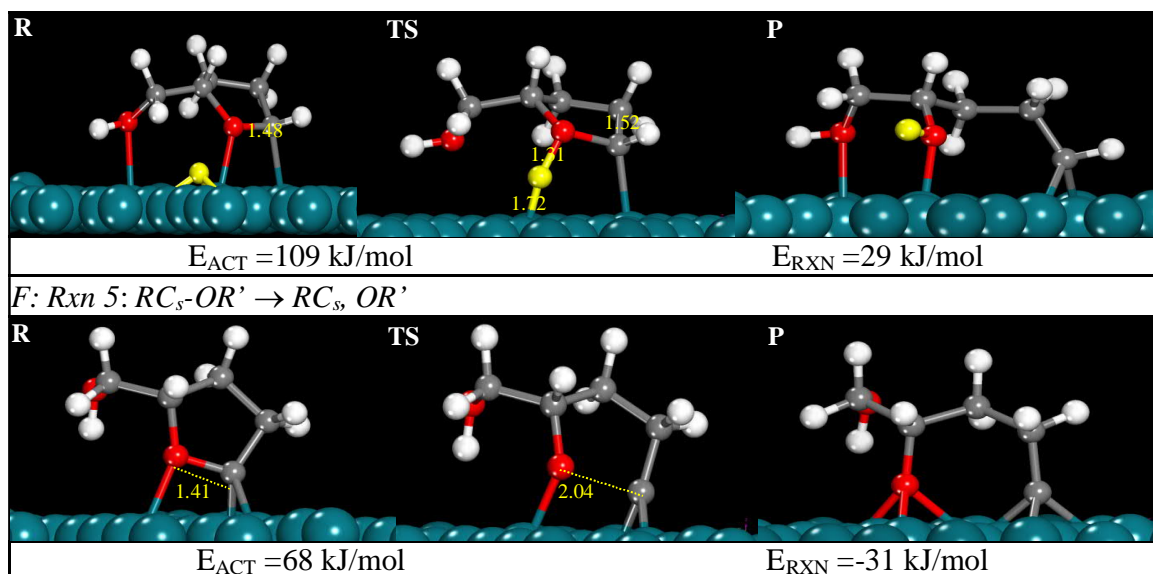


Figure 4. Initial, transition and final state geometries for the dehydrogenation and ring opening reactions of *THFA* over the secondary carbon.

The activation of the C-O bond is thought to proceed subsequent to the activation of the C-H bonds. The direct activation of the C-O bond of the C-adsorbed intermediate  $RC_sH-OR'$  intermediate on the Rh (111) surface is shown in Fig. 4C (*Rxn 4*). We can see that the C-O bond elongates from 1.48 Å to 2.78 Å in the transition state. And in the transition state geometry, the three bonds that associated with the secondary carbon atom of the C-O bond are in the same plane indicating that the carbon atom is  $sp^2$  hybridized. The calculated barrier for this reaction is 85 kJ/mol which is higher than the barriers (53 and 72 kJ/mol) to activate the secondary C-H bonds. The reaction energy for C-O activation was calculated to be slightly endothermic with a reaction energy of 9 kJ/mol. The activation of the secondary C-O of  $RC_sH-OR'$  can also proceed with the assistance of co-adsorbed hydrogen atoms via a concerted step where the C-O bond breaks as hydrogen is added to the carbon or the oxygen. The H\*-assisted ring-opening of  $RC_sH-OR'$  that proceeds at the carbon of the C-O bond is shown in Fig. 4D (*Rxn 7*). The C-O distance

increases by 0.68 Å from 1.48 Å to 2.16 Å in the transition state, which is significantly less than 1.32 Å increase in the transition state reported for the direct C-O cleavage step. The H atom inserts to form the classic three-center transition state complex shown in Figure 4D. The activation energy for this reaction is 128 kJ/mol which is considerably higher than the two-step activation barrier of 85 kJ/mol for the direct ring-opening of the  $RC_sH-OR'$  intermediate followed by its subsequent hydrogenation, as shown in Fig. 3 (*Rxns 4→15*).

The H\*-assisted ring-opening of  $RC_sH-OR'$  by concurrently hydrogenating the oxygen of the C-O bond is shown in Fig. 4E (*Rxn 8*). We can see that the hydrogen inserts into the O-Rh bond and the C-O bond elongates slightly from 1.48 Å to 1.51 Å. The activation energy for this reaction is 109 kJ/mol which is also considerably higher than that for the direct ring-opening reaction followed by hydrogenation (in this case of the O atom) which was only 95 kJ/mol. The hydrogenation of the strongly adsorbed oxygen atom resulted in the highest barrier in the two-step process which is shown in Fig. 3 (*Rxns 4→16*). We can conclude that at low H\* coverages the direct ring-opening pathways are preferred to H-assisted pathways. However, under the experimental conditions, it is likely that there are higher coverages of H\* on the surface. Among other effects, we would expect that the direct ring-opening pathways would become more difficult, whereas H-assisted ring-opening would become more facile. As such, more detailed studies of coverage effects are needed to establish the dominant path under working conditions. Similar to the ring opening of the C-adsorbed  $RC_sH-OR'$  intermediate, there are three possible paths associated with the activation of the C-O bond and ring opening of the  $RC_s-OR'$  intermediate. In the direct ring-opening of  $RC_s-OR'$ , the C-O bond elongates from 1.41 Å to 2.01 Å in the transition state and the carbon becomes  $sp^2$  hybridized as is shown in Fig. 4F (*Rxn*

6) and similar to that which was found in the direct ring-opening of  $RC_sH-OR'$ . The activation barrier for the direct ring opening of  $RC_s-OR'$  was calculated to be 68 kJ/mol, which is 17 kJ/mol lower than that of the direct ring-opening reaction of  $RC_sH-OR'$ . The lower barrier for the path through  $RC_s-OR'$  is the result of the much stronger binding of the alkylidyne group to the metal that results in the transition state in the  $RC_s-OR'$  ring-opening reaction than the weaker binding of the alkylidene group to the metal in the transition state for the ring-opening reaction of  $RC_sH-OR'$  intermediate.

The H\*-assisted ring-opening paths for the  $RC_s-OR'$  intermediate were also analyzed. The path involving the ring-opening activation of the C-O bond and the concurrent addition of hydrogen to the oxygen is shown in the Appendix. The activation energy for this step is 130 kJ/mol, which is much higher than the overall activation energy of the two-step pathway (*Rxns 5→14*) involving the direct ring-opening followed by hydrogenation which was calculated to be 70 kJ/mol. The transition state for the H\*-assisted ring-opening of  $RC_s-OR'$  and concurrent addition of hydrogen to the carbon could not be isolated or forced by NEB methods as the minimum path always proceeded instead through a direct ring-opening step followed by the subsequent hydrogenation, indicating that the two-step pathway is much more favorable. The calculated two-step path was found to have an overall activation barrier of 71 kJ/mol as shown in Fig. 3 (*Rxns 5→13*). Similar to the ring opening of the  $RC_sH-OR'$ , we can conclude that both H-assisted ring-opening pathways for the  $RC_s-OR'$  are unfavorable compared to the direct ring-opening pathway at low H\* coverages.

The hydrogenation of the direct-ring opened  $RC_s-OR'$  products can proceed through various

routes to form the diol products. Both  $RC_5H-OHR'$  and  $RC_5-OR'$  proceed through direct ring opening followed by hydrogenation. To determine which of these paths is the most favorable path, we compare the single direct ring-opening step of the  $RC_5H-OR'$  (*Rxn 4*) intermediates (shown in red) to the three-step sequence required for the opening of the  $RC_5-OR'$  intermediate (*Rxns 2*→*5*→*13* shown in black) in Fig. 5. The dehydrogenation step and the ring-opening step of the multi-step pathway are exothermic which offsets the somewhat higher activation energies for hydrogenation step so that the overall activation energy for the multi-step pathway is 53 kJ/mol which is 35 kJ/mol lower than the one-step path at 85 kJ/mol. This indicates that the C-O bond of the ring ether is completely dehydrogenated prior to the ring-opening C-O activation. This is consistent with the results reported for the hydrogenolysis of cyclic hydrocarbons which demonstrate that the activation of a  $-CH_2-CH_2-$  bond occurs after the adsorption and activation of the four C-H bonds to form the  $\alpha,\alpha,\beta,\beta$ -tetra-adsorbed species.<sup>22</sup>

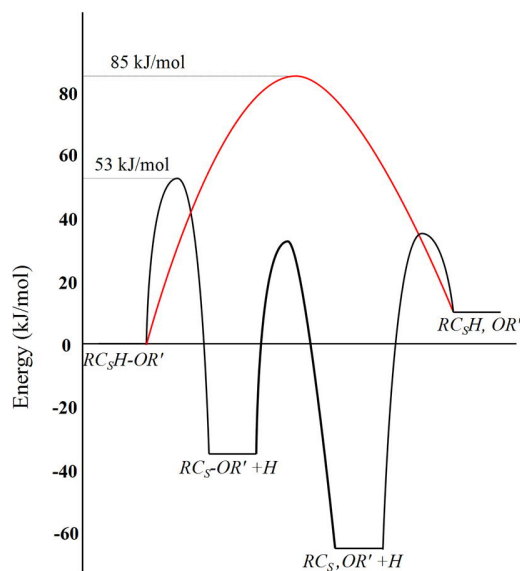


Figure 5. Reaction energy diagram comparing the direct single step ring-opening of the  $RC_5H-OR'$  (*Rxn 3*) shown in red to the three step path for the  $RC_5-OR'$  intermediate (*Rxns 2*→*5*→*13*) shown in black; the energies are reported in kJ/mol.

The ring opening of  $RC_5-OR'$  results in the formation of  $RC_5,OR'$  surface intermediates that can be hydrogenated to form the final  $1,2-PDO$  product via three C-atom hydrogen additions and a single O-atom hydrogen addition. Four pathways can be constructed, by varying the sequence of the different hydrogenation reactions as shown in Fig. 6. These are presented and discussed in detail in the Appendix. The most preferred path involves the three C-Atom hydrogen additions followed by the single and final O-atom hydrogen addition resulting in an overall barrier of 135 kJ/mol as shown in Fig. 6.

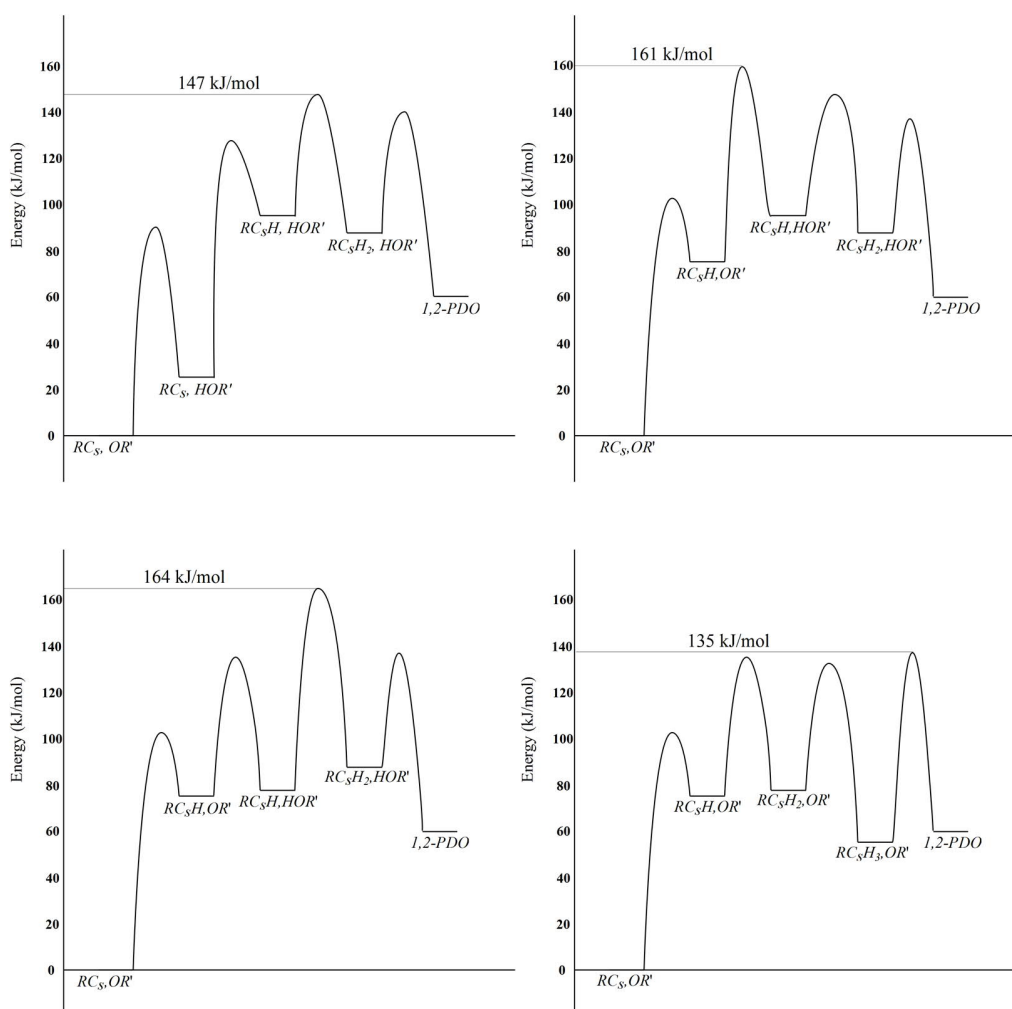


Figure 6. Energy diagrams for the four different pathways of the hydrogenation process from  $RC_5,OR'$  to  $1,2-PDO$ .

We summarize the energetics for all of the elementary steps in the most favorable (lowest energy) path for the hydrogenolysis of *THFA* to *1,2-PDO* in reaction energy diagram shown in Fig. 7. The overall activation energy for the hydrogenolysis of *THFA* to form *1,2-PDO* is 72 kJ/mol in reference to the adsorbed *THFA* ( $E_{\text{ads}} = -44$  kJ/mol). The first step in this path which involves the activation of the C-H bond of the secondary C of the C-O bond of *THFA* has the highest energy, suggesting it is possible to be the rate-limiting step for this reaction. The potential energy surface also shows that the ring-opened  $RC_sOR'$  is very strongly held to the surface and has an intrinsic barrier to hydrogenate that is 90 kJ/mol which would suggest that it can readily build up on the surface. The surface coverages of  $RC_sOR'$  or hydrogen that exist under operate conditions are likely much higher than those examined here. This would suggest that the dehydrogenation and ring-opening reactions would become more difficult whereas the hydrogenation steps would become more feasible.

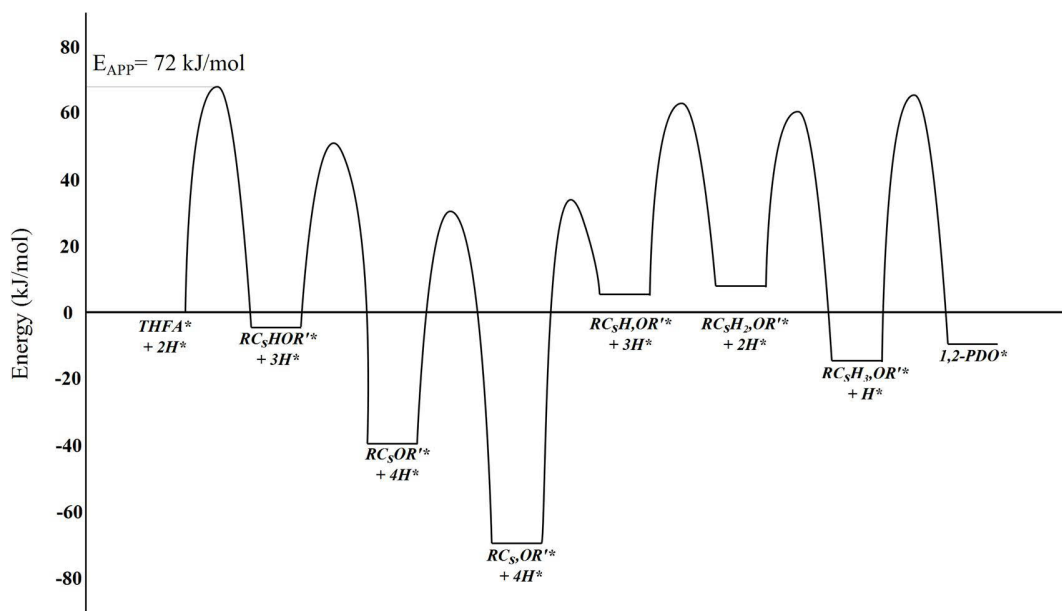


Figure 7. Most favorable potential energy path for the hydrogenolysis of adsorbed *THFA* at the secondary carbon to *1,2-PDO* over Rh(111).

To further understand the kinetics of the whole hydrogenolysis process, other methods such as Kinetic Monte Carlo simulations<sup>50</sup> will be used and the energetics for the elementary steps we showed here can be used as the inputs for the Kinetic Monte Carlo simulations, and will be shown in the future publication.

### 3.3 Hydrogenolysis of THFA to form 1,5-PDO

The reactant, transition and product states involved in the activation of the C-H bond at the more substituted tertiary carbon of THFA to form the C-adsorbed intermediate  $RO-C_3R'$  is shown in Fig. 8A (Rxn 3). While the transition state structure for the activation of this tertiary C-H bond is quite similar to that for secondary C-H bond associated with the C-O ether linkage, the activation barrier is 87 kJ/mol which is 15 kJ/mol higher than that for the activation of the C-H bond of the secondary carbon due to the repulsive steric interactions that result from the  $-CH_2OH$  substitute of the tertiary carbon. Similar substituent effects were also observed in glycerol hydrogenolysis on Rh (111) surface in which the C-H activation over the more-substituted carbon has a higher energy barrier than the less-substituted terminal carbon.<sup>47</sup> These steric interactions also lead to a small elongation of the C-Rh bond in the transition state from 2.23 Å for C-H activation at the secondary carbon to 2.36 Å for the C-H activation at the tertiary carbon.

The C-adsorbed  $RO-C_3R'$  intermediate can undergo either direct ring-opening on the surface or H\*-assisted ring-opening, similar to  $RC_3H-OR'$  and  $RC_3-OR'$  activation, previously discussed. The direct ring opening proceeds via elongation of the C-O bond from 1.48 Å in the adsorbed

state to 2.82 Å in the transition state as is shown in Fig 8B (*Rxn 6*) which is very similar to the structure for the direct ring-opening of  $RC_5H-OR'$  shown in Fig. 4C (*Rxn 4*). The activation energy of this reaction is calculated to be 93 kJ/mol, which is ~8 kJ/mol higher than the barrier for the direct ring-opening of  $RC_5H-OR'$ . The higher barrier associated with activating the C-O bond for  $RO-C_7R'$  is likely also the result of steric constraints of the substituent on the binding of C to the surface which is indicated by the longer C-Rh distance in the transition state for  $RO-C_7R'$  (1.93 Å) than that for  $RC_5H-OR'$  (1.89 Å).

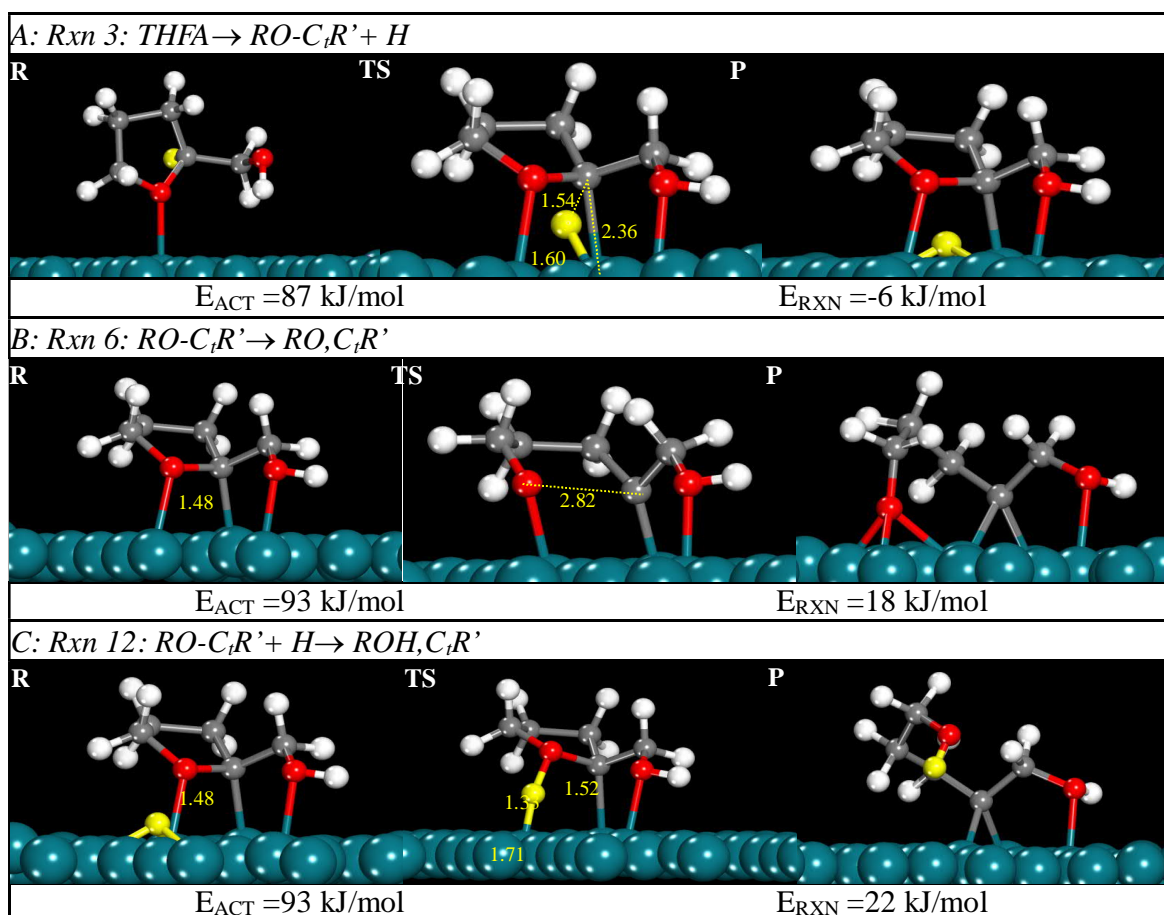


Figure 8. Initial, transition and final state structures for the dehydrogenation and ring opening reactions of *THFA* over the tertiary carbon.

A comparison of the activation energies for direct ring-opening of  $RC_s-OR'$ ,  $RC_sH-OR'$  and  $RO-C_tR'$  indicate that they are directly correlated to the energies of reaction in a classic Brønsted-Evans-Polyani (BEP) relationship as is shown in Figure 9A. The changes in the activation energies between species are directly related to the changes in the adsorption energies of the  $RC_s-OR'$ ,  $RC_sH-OR'$  and  $RO-C_tR'$  structures which are directly tied to the binding of the RC-, RCH- and RR'C- groups and the surface. The stronger the carbon group binds to the surface, the lower the reaction and activation energies of the ring-opening reaction.

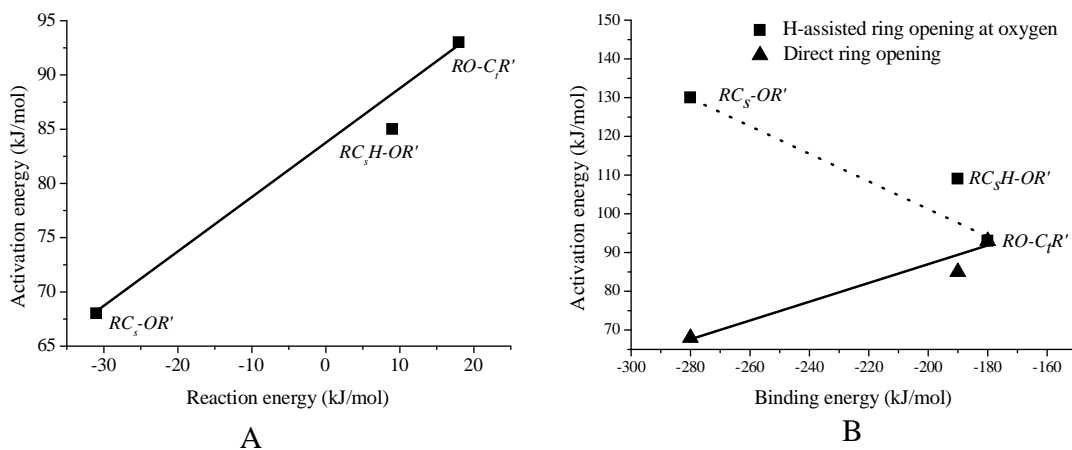


Figure 9. Brønsted-Evans-Polyani relationship between the activation barriers and the overall reaction energies for the direct ring-opening of  $RC_s-OR'$ ,  $RC_sH-OR'$  and  $RO-C_tR'$  intermediates (A) and the correlation of the of the activation energies for the direct ring opening and the H\*-assisted ring opening and the binding energies (B) of the three C-bound species  $RC_sH-OR'$ ,  $RC_s-OR'$  and  $RO-C_tR'$ .

The H-assisted ring-opening of the  $RO-C_tR'$  intermediate was also examined and the resulting reaction path associated with the addition of hydrogen to the carbon and ring opening at the

tertiary C-O bond is shown in the Appendix. The activation energy for this path was calculated to be 135 kJ/mol, which is much higher than the two-step path (*Rxns 6*→*23*). This is very similar to results for H-assisted ring-opening reactions reported earlier. The H-assisted ring-opening of *RO-C<sub>i</sub>R'* by the concurrent addition of hydrogen to oxygen, however, was found to have a much lower barrier, 93 kJ/mol, as shown in Fig 8C (*Rxn 12*). Similar to the previously discussed hydrogen-assisted ring opening reactions, hydrogen inserts into the O-Rh bond which weakens the C-O bond increasing the C-O distance from 1.48 Å to 1.53 Å in the transition state. Unlike the previous cases, the direct ring opening two-step path (*Rxns 6*→*24*) has a higher overall activation barrier (115 kJ/mol) than the H-assisted path (93 kJ/mole) which is the result of the high endothermicity of the direct ring-opening reaction and the high barrier of the subsequent hydrogenation. The barrier for the hydrogen assisted path is 22 kJ/mol lower than that for the direct ring opening which indicates that H\* assists in ring-opening hydrogenolysis of the *RO-C<sub>i</sub>R'* intermediate, even at the low H\* coverage modeled in this work.

Examining all three H-assisted ring-opening reactions in which the oxygen is concurrently hydrogenated, it was found that as the binding strength of the carbon-bound intermediate decreases, the direct ring-opening path becomes more difficult and the H-assisted ring-opening becomes more facile as shown in Fig. 9B. We can see from Fig. 9B that for the three C-adsorbed species, the ring-opening of *RO-C<sub>i</sub>R'* is the only path which proceeds more favorably by the H-assisted ring-opening (via hydrogen addition to the oxygen) over the direct ring-opening path. It is worth noting, however, that the calculations reported in this study were all carried out at low H\* coverage. As discussed earlier, high coverages will act to increase the barriers for dissociation while decreasing the barriers for association reactions.<sup>48</sup> Thus at higher H\*

coverages, it is very likely that the barriers for the direct ring-opening pathways will increase while the barriers for the H-assisted ring-opening paths will decrease, thus making them more favorable.

The  $ROH, C_tR'$  that forms as a result of the H-assisted ring-opening subsequently undergoes two hydrogen addition steps to hydrogenate the strongly bound secondary carbon at the bridging metal site and form  $1,5-PDO$ , ( $Rxns\ 27 \rightarrow 29$ ). The barriers for forming the first and second C-H bond were calculated to be 59 and 69 kJ/mol, respectively. We examined various other possible hydrogenation pathways for the C-bound intermediate,  $RO-C_tR'$  as shown in details in the Appendix, but all of these paths had higher overall energy barriers.

The lowest energy dehydrogenation, C-O bond breaking and the hydrogenation steps were combined together to construct the most favorable path for the hydrogenolysis of  $THFA$  over the tertiary carbon to form  $1,5-PDO$  which is presented in Fig. 10. This path proceeds by the initial C-H activation of the tertiary C-O carbon of  $THFA$  to form the C-bound  $RO-C_tR'$  intermediate, which will then ring-opens via a H-assisted mechanism in which the C-O bond concertedly breaks as hydrogen adds to the oxygen. The resulting  $ROH, C_tR'$  intermediate undergo two hydrogen additions to saturate the bound secondary carbon atom to the final product  $1,5-PDO$ . The overall activation energy for this path referenced to adsorbed  $THFA$  which is 92 kJ/mol is the result of the final hydrogenation addition to the carbon-bound  $ROH, C_tR'$  intermediate. However, at higher  $H^*$  coverages, it is expected that the hydrogen addition barriers would decrease while the C-H and C-O activation reactions would increase. As such the overall activation energy for the H-assisted ring opening reaction examined here which is governed by

the final hydrogenation steps would decrease at higher  $H^*$  coverages. Therefore, it is speculated that under experimental conditions, the rate-limiting step may actually be the initial dehydrogenation of the tertiary carbon, which, as was discussed, is 15 kJ/mol higher than the initial activation of the secondary carbon, due to steric effects of the  $-CH_2OH$  substituent. This is consistent with experiments which indicate that the selectivity to form *1,2-PDO* is slightly higher than the selectivity forming *1,5-PDO* on Rh/SiO<sub>2</sub> catalysts, although those selectivity measurements are complicated by further hydrogenolysis of the diols to mono-alcohols and gas-phase products (presumably alkanes and CO<sub>2</sub>).

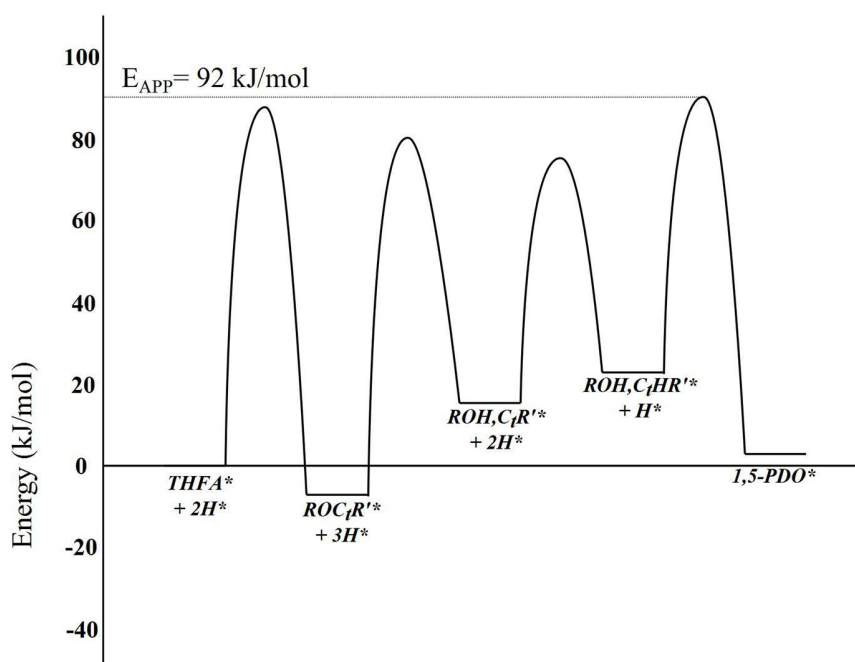


Figure 10. Most favorable potential energy path for the hydrogenolysis of adsorbed *THFA* at the tertiary carbon to *1, 5-PDO* over Rh(111).

## Chapter 4 - Conclusions

First principle density functional theory calculations were carried to systematically examine the possible pathways that control the hydrogenolysis of *THFA* over a Rh (111) surface, and determine the most plausible paths to form the *1,2-PDO* and *1,5-PDO* products. The results indicate that all the C-H bonds on the ether carbon of *THFA* are broken before the corresponding C-O bond breaks. And the C-H bond activation at the less substituted secondary carbon is easier than the more substituted carbon, which is consistent with the cyclic hydrocarbons reported. Hydrogen adsorbed at the metal surface can assist the C-O activation of the intermediates after C-H activations of *THFA*. At the secondary carbon, the direct C-O activation paths are preferred to the H assisted C-O activation paths, while at the more substituted tertiary carbon, the H-assisted C-O activation is more favorable via the H addition to the ether oxygen. The C-O activation at the secondary carbon has lower energy barrier than at the tertiary carbon. Comparison of the two different pathways of the hydrogenolysis of *THFA* towards *1,2-PDO* and *1,5-PDO* shows that the overall activation energy for the hydrogenolysis at the less substituted secondary C-O bond to form *1,2-PDO* is ~20 kJ/mol lower than the overall activation energy for the hydrogenolysis at the more substituted tertiary carbon-O bond to form *1,5-PDO* which can help to explain the higher selectivity to *1,2-PDO* rather than *1,5-PDO* over Rh catalysts reported experimentally. The results reported herein suggest that H\* on the surface can influence the barriers for C-H activation, C-O bond scission and the hydrogen addition reactions involved in the hydrogenolysis of *THFA*, thus the effect of H\* coverage in the hydrogenolysis of *THFA* is currently being examined and will be the subject of a future publication.

## References

1. Huber, G. W.; Chheda, J. N.; Barrett, C. J.; Dumesic, J. A. Production of liquid alkanes by aqueous-phase processing of biomass-derived carbohydrates, *Science* 2005, 308, 1446.
2. Chheda, J. N.; Huber, G. W.; Dumesic, J. A. Liquid phase catalytic processing of biomass derived oxygenated hydrocarbons to fuels and chemicals, *Angewandte Chemie International Edition* 2007, 46, 7146.
3. Huber, G. W.; Iborra, S.; Corma, A. Synthesis of transportation fuels from biomass: chemistry, catalysts, and engineering, *Chemical Review* 2006, 106, 4044.
4. Corma, A.; Iborra, S.; Velty, A. Chemical routes for the transformation of biomass into chemicals, *Chemical Review* 2007, 107, 2411.
5. Schlaf, M. Selective deoxygenation of sugar polyols to  $\alpha,\omega$ -diols and other oxygen content reduced materials-a new challenge to homogeneous ionic hydrogenation and hydrogenolysis catalysis, *Dalton Transactions* 2006, 39, 4645.
6. Gallezot, P. Process options for converting renewable feedstocks to bioproducts, *Green Chemistry* 2007, 9, 295.
7. Corma, A.; Huber, G. W. L. Sauvinaud and P. O'Connor, Biomass to chemicals: Catalytic conversion of glycerol/water mixtures into acrolein, reaction network, *Journal Catalysis* 2008, 257, 163.
8. Gallezot, P. Catalytic conversion of biomass: challenges and issues, *ChemSusChem* 2008, 1, 734.

9. Coll, D.; Delbecq, F.; Aray, Y.; Sautet, P. Stability of intermediates in the glycerol hydrogenolysis on transition metal catalysts from first principles, *Physical Chemistry Chemical Physics* 2011, 13, 1448.
10. Nakagawa, Y.; Shinmi, Y.; Koso, S.; Tomishige, K. Direct hydrogenolysis of glycerol into 1,3-propanediol over rhenium-modified iridium catalyst, *Journal of Catalysis* 2010, 272, 191.
11. Shinmi, Y.; Koso, S.; Kubota, T.; Nakagawa, Y.; Tomishige, K. Modification of Rh/SiO<sub>2</sub> catalyst for the hydrogenolysis of glycerol in water, *Applied Catalysis B: Environmental* 2010, 94, 318.
12. Maris, E. P.; Davis, R. J. Hydrogenolysis of glycerol over carbon-supported Ru and Pt catalysts, *Journal of Catalysis* 2007, 249, 328.
13. Olcay, H.; Xu, L.; Xu, Y.; Huber, G. W. Aqueous phase hydrogenation of acetic acid over transition metal catalysts, *ChemCatChem*, 2010, 2, 1420.
14. Pham, T. T.; Lobban, L. L.; Resasco, D. E.; Mallinson, R. G. Hydrogenation and hydrodeoxygenation of 2-methyl-2-pentenal on supported metal catalysts, *Journal of Catalysis* 2009, 266, 9.
15. Lahr, D. G.; Shanks, B. H. Kinetic analysis of the hydrogenolysis of lower polyhydric alcohols: glycerol to glycols, *Industrial & Engineering Chemistry Research* 2003, 42, 5467.
16. Wang, K.; Hawley, M. C.; Furney, T. D. Mechanism Study of Sugar and Sugar Alcohol Hydrogenolysis Using 1,3-Diol Model Compounds, *Industrial & Engineering Chemistry Research* 1995, 34, 3766.
17. Lichtenthaler, F. W. Unsaturated O- and N-Heterocycles from Carbohydrate Feed-stocks, *Accounts of Chemical Research* 2002, 35, 728.

18. Koso, S.; Furikado, I.; Shima, A.; Miyazawa, T.; Kunimori, K.; Tomishige, K. Chemoselective hydrogenolysis of tetrahydrofurfuryl alcohol to 1, 5-pentanediol, *Chemical Communications* 2009, 15, 2035.
19. Chia, M.; Pagan-Torres, Y. J.; Hibbitts, D.; Tan, Q.; Pham, H. N.; Datye, A. K.; Neurock, M.; Davis, R. J.; Dumesic, J. A. Selective hydrogenolysis of polyols and cyclic ethers over bifunctional surface sites on rhodium-rhenium catalysts, *Journal of American Chemical Society* 2011, 133, 12675.
20. Gault, F. G.; Effect of the dispersion of platinum catalyst on the hydrogenation of cyclopentane hydrocarbons, *Comptes Rendus* 1957, 245, 1620.
21. Gault, F. G. Hydrogenolysis of cyclopentane hydrocarbons, *Annales de Chimie. (Paris)* [13] 1960, 5, 645.
22. Maire, G.; Plouidy, G.; Prudhomme, J. C.; Gault, F. G. The mechanisms of hydrogenolysis and isomerization of hydrocarbons on metals. I. Hydrogenolysis of cyclic hydrocarbons, *Journal of Catalysis* 1965, 4, 556.
23. Corolleur, C.; Muller J. M.; Gault, F. G. Proc. Meet. Soc. Chim. Phys., 20th. Paper.
24. Weisang, F.; Gault, F. G. Selective isomerization of methylpentanes on iridium catalysts, *Journal of the Chemical Society, Chemical Communications* 1979, 11, 519.
25. Maire, G.; Gault, F. G. Hydrogenolysis and isomerization mechanisms of hydrocarbons on metals. III. Hydrogenolysis of cis- and trans-1, 2-dimethylcyclobutanes, *Bulletin de Societe Chimique de France* 1967, 3, 894.
26. Kemball, C. The reaction of methane and deuterium on evaporated nickel catalysts, *Proceedings of the Royal Society of London, Series A* 1951, 207, 539.

27. Amir-Ebrahimi, V.; Garin, F.; Weisang F.; Gault, F. G. Mechanisms of skeletal isomerization of hydrocarbons on metals, *Nouveau Journal de Chimie* 1979, 3, 529.
28. Anderson, J. R.; Kemball, C. Catalysis on evaporated metal films. V. Reactions between cyclic hydrocarbons and deuterium, *Proceedings of the Royal Society of London, Series A* 1954, 226, 472.
29. Burwell, R. L.; Shim; B. K. S.; Rowlinson, H. C. Exchange between hydrocarbons and deuterium on palladium catalysts, *Journal of American Chemical Society* 1957, 79, 5142.
30. Gennari, U.; Kramer, R. Gruber, H. L. Hydrogenolysis of methyltetrahydrofuran on platinum, *Applied Catalysis* 1984, 11, 341-351.
31. Gennari, Kramer, U. R.; Gruber, H. L. Hydrogenolysis of methyltetrahydrofuran on platinum. II. Effects of self-poisoning and evaluation of structure sensitivity, *Applied Catalysis* 1988, 44, 239-250.
32. Kreese G.; Hafner, J. Ab initio molecular dynamics of liquid metals, *Physical Review B* 1993, 47, 558.
33. Kohn W.; Sham, L. Quantum density oscillations in an inhomogeneous electron gas, *Physical Review* 1965, 137, 1697
34. Perdew, J. P.; Chevery, J. A.; Vosko, S. H.; Jackson, K. A.; Pederson, M. R.; Singh, D. J.; Fiolhais, C. Atoms, molecules, solids, and surfaces: applications of the generalized gradient approximation for exchange and correlation, *Physical Review B* 1992, 46, 6671.
35. Vanderbilt, D. Optimally smooth norm-conserving pseudopotentials, *Physical Review B* 1985, 32, 8412.
36. Monkhorst, H. J.; Pack, J. D. On special points for Brillouin Zone integrations, *Physical Review B* 1976, 13, 5188.

37. Henkelman G.; Jonsson, H. A dimer method for finding saddle points on high dimensional potential surfaces using only first derivatives, *Journal of Chemical Physics* 1999, 111, 7010.
38. Heyden, A.; Bell, A. T.; Keil, F. J. Efficient methods for finding transition states in chemical reactions: Comparison of improved dimer method and partitioned rational function optimization method, *Journal of Chemical Physics* 2005, 123, 224101.
39. Kaestner, J.; Sherwood, P. Superlinearly converging dimer method for transition state search, *Journal of Chemical Physics* 2008, 128, 014106.
40. Mills, G.; Jonsson, H.; Schenter, G. K. Reversible Work Transition-State Theory-Application to Dissociative Adsorption of Hydrogen, *Surface Science* 1995, 324, 305.
41. Jónsson, H.; Mills, G.; Jacobsen, K.W. Nudged elastic band method for finding minimum energy paths of transitions, *Classical and Quantum Dynamics in Condensed Phase Simulations*, World Scientific, Singapore, 1998, 385.
42. Henkelman G.; Jonsson, H. Improved tangent estimate in the nudged elastic band method for finding minimum energy paths and saddle points, *Journal of Chemical Physics* 2000, 113, 9978.
43. Sheppard, D.; Terrell, R.; Henkelman, G. Optimization methods for finding minimum energy paths, *Journal of Chemical Physics* 2008, 128, 134106.
44. *CRC Handbook of Chemistry and Physics*, 76th ed.; Lide, D. R., Ed.; CRC Press: New York, 1996.
45. Thierfelder, C.; Schmidt, W. G. First-principles study of water adsorption and a high-density interfacial ice structure on (1x1)-O/Rh(111), *Physical Reviews B* 2010, 82, 115402.
46. Alcala, R.; Mavrikakis, M.; Dumesic, J. A. DFT studies for cleavage of C-C and C-O bonds in surface species derived from ethanol on Pt(111), *Journal of Catalysis* 2003, 218, 178.

47. Neurock, M.; Pallassana, V.; Santen, R. A. The importance of transient states at higher coverages in catalytic reactions, *Journal of American Chemical Society* 2000, 122, 1150.
48. Bunnik, B. S.; Kramer, G. J. Energetics of methane dissociative adsorption on Rh{111} from DFT calculations, *Journal of Catalysis* 2006, 242, 309.
49. Auneau, F.; Michel, C.; Delbecq, F.; Pinel, C.; Sautet, P. Unravelling the mechanism of glycerol hydrogenolysis over rhodium catalyst through combined experimental-theoretical investigations, *Chemistry- A European Journal* 2011, 17, 14288.
50. Mei, D.; Neurock, M.; Smith, M. C. Hydrogenation of acetylene-ethylene mixtures over Pd and Pd-Ag alloys: First-principles-based kinetic Monte Carlo simulations. *Journal of Catalysis* 2009, 268, 181.

## Appendix

In this chapter, the initial, transition and final state in the hydrogenolysis of *THFA* to form *1,2-PDO* and *1,5-PDO*, which are not shown in Chapter 3 are shown here in Fig. A1, A2 and A3. Reaction energy diagrams comparing the H assisted ring opening pathways and the direct ring opening pathways in the ring opening of the C-adsorbed intermediates  $RC_sH-OR'$ ,  $RC_s-OR'$  and  $RO-C_tR'$  are shown in Fig. A4. The reaction energy diagrams for the other two pathways of the hydrogenation of  $RO$ ,  $C_tR'$  towards *1,5-PDO* are shown in Fig. A5.

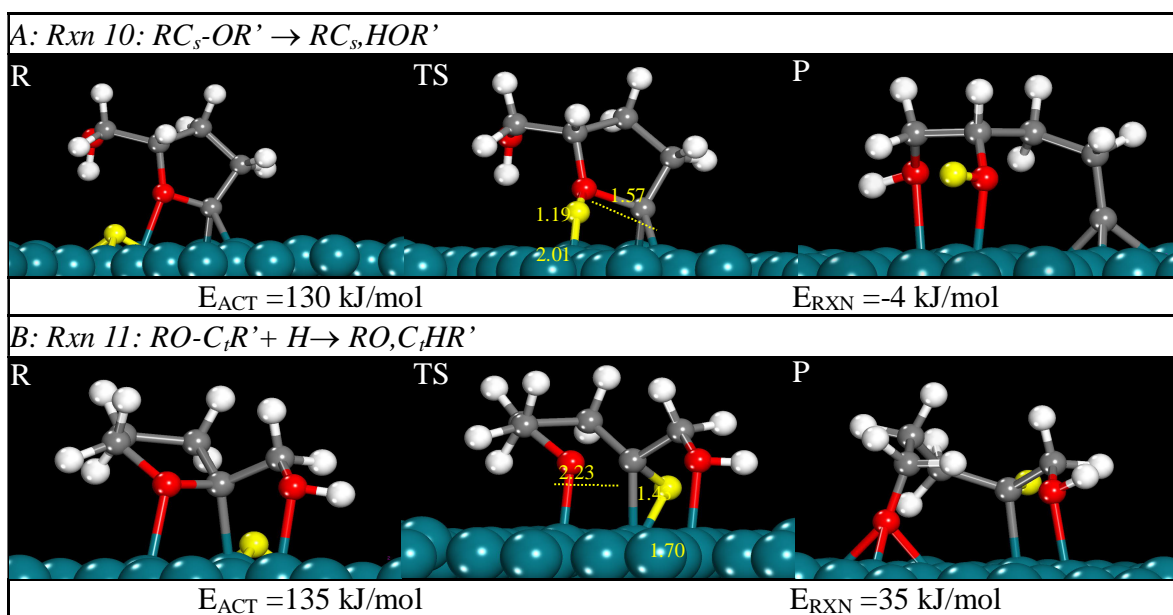
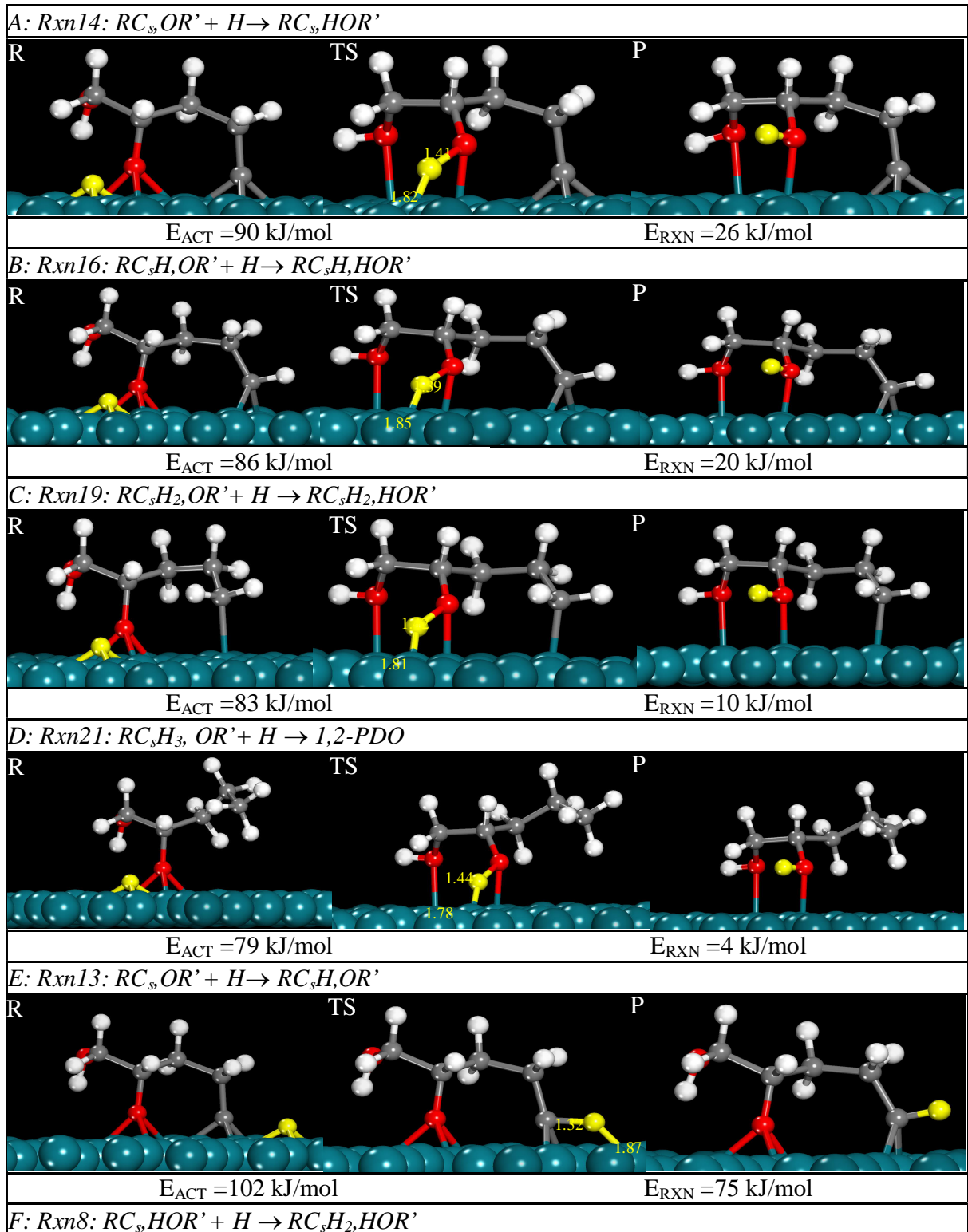


Figure A1. Initial, transition and final state of the H assisted ring opening of the C-adsorbed species  $RC_s-OR'$  and  $RO-C_tR'$  not shown in Chapter 3.



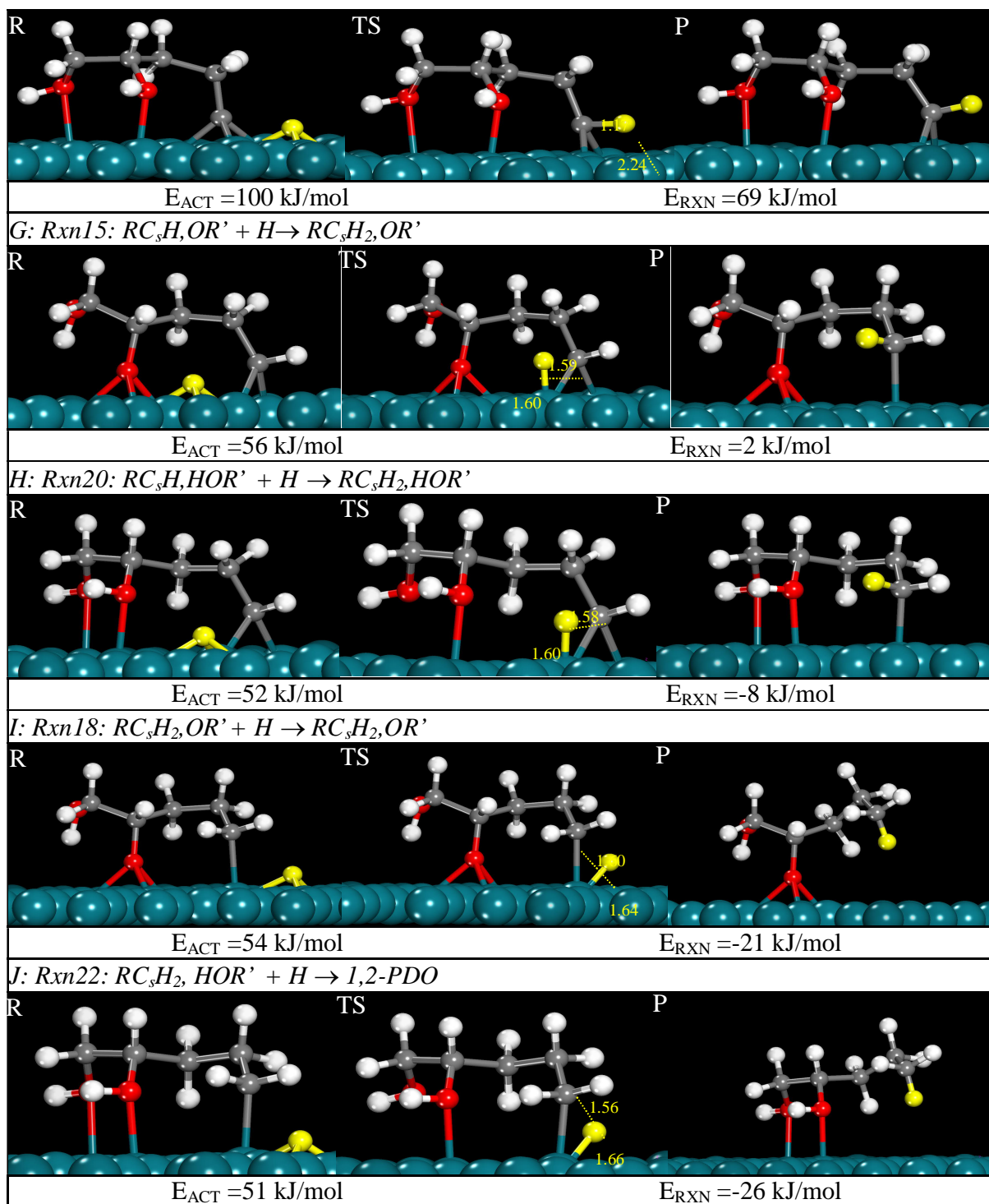
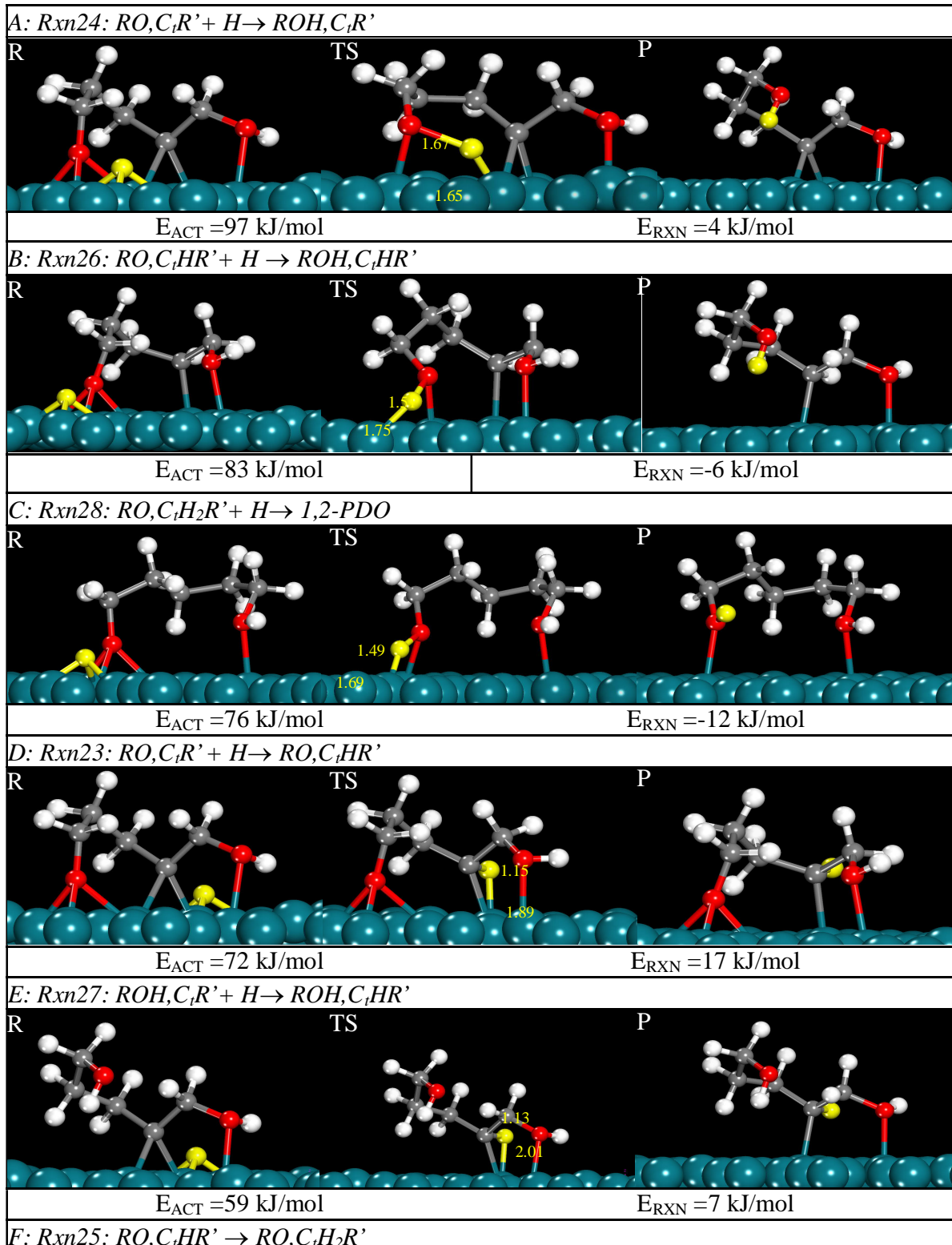


Figure A2. Initial, transition and final states of the reactions involved in the hydrogenation of  $RC_5, OR'$  towards 1,2-PDO.



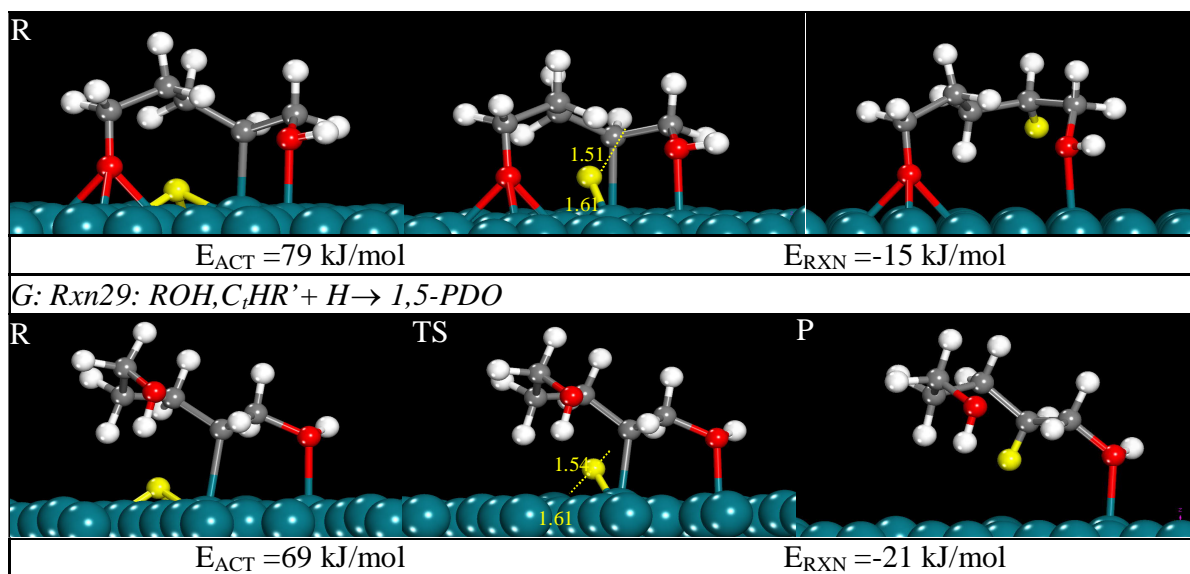


Figure A3. Initial, transition and final state of the reactions involved in the hydrogenation of  $RO$ ,  $C_iR'$  towards  $1,5\text{-PDO}$ .

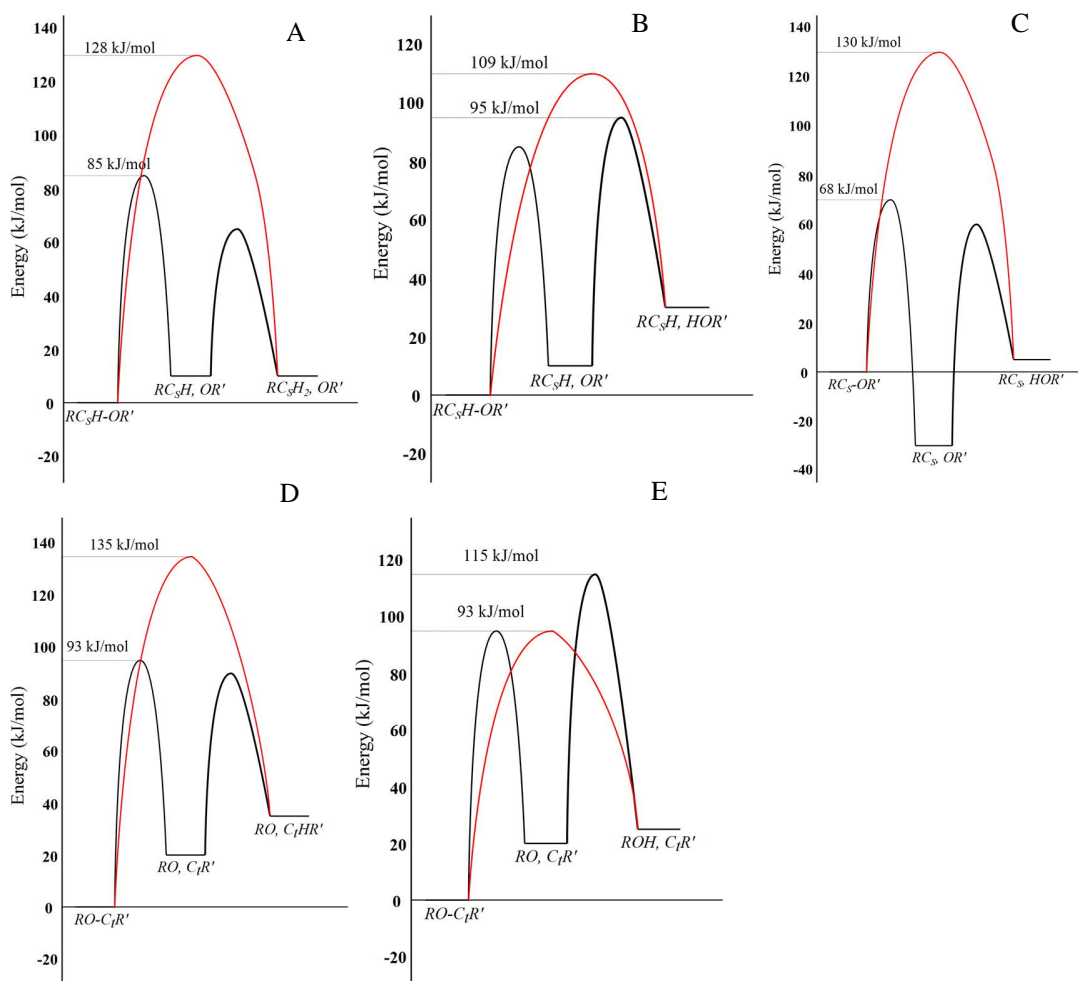


Figure A4. Reaction energy diagrams comparing the H assisted ring opening pathways and the direct ring opening pathways in the ring opening reactions of the C-adsorbed species: (A) H-assisted ring opening of  $RC_3H-OR'$  with H addition to carbon; (B) H-assisted ring opening of  $RC_3H-OR'$  with H addition to oxygen; (C) H-assisted ring opening of  $RC_5-OR'$  with H addition to oxygen; (D) H-assisted ring opening of  $RO-C_1R'$  with H addition to carbon; (E) H-assisted ring opening of  $RO-C_1R'$  with H addition to oxygen.

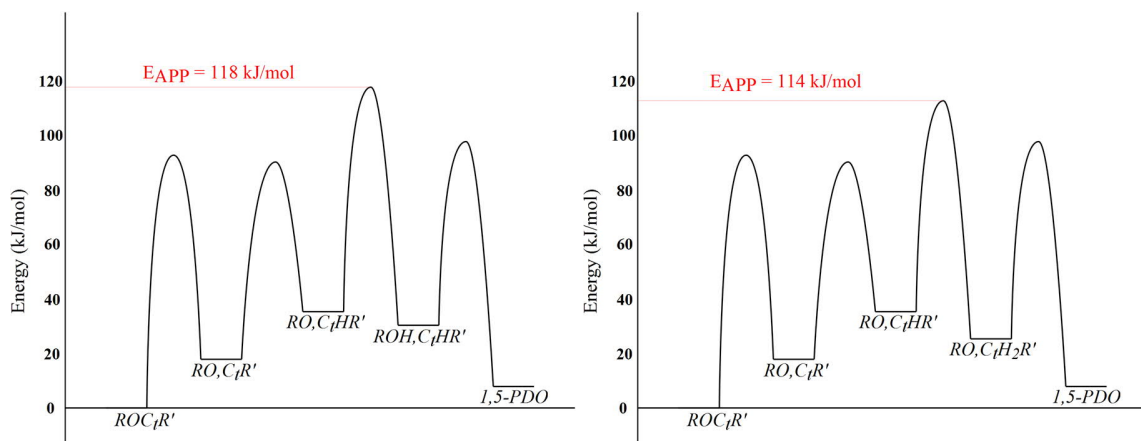


Figure A5. Reaction energy diagrams for the two different paths for the hydrogenation of  $RO-C_1R'$  to form  $1,5-PDO$ .